https://doi.org/10.1016/j.compositesb.2017.03.028

Surface Charge Switchable and pH-responsive Chitosan/Polymer Core-Shell Composite Nanoparticles for Drug Delivery Application

[1]W.F. Huang, *[1]C.P. Tsui, [1]C.Y. Tang, [2]M. Yang, [3]Linxa Gu

[1]Department of Industrial and Systems Engineering, The Hong Kong Polytechnic University, Hung Hom, Kowloon, Hong Kong, China

[2]Interdisciplinary Division of Biomedical Engineering, The Hong Kong Polytechnic University, Hung Hom, Kowloon, Hong Kong, China

[3]Department of Mechanical and Materials Engineering, University of Nebraska-Lincoln, NE 68588-0656, USA

Abstract

The mutually conflicting surface charge requirements for nanoparticles to have long circulation and good cell affinity have made the development of polymer nanoparticles for controlled drug delivery fall into a dilemma. In order to solve this problem, the first attempt has been made in this work to develop vancomycin loaded composite nanoparticles with a novel chitosan core and poly (lactide-co-glycolide) (PLGA) shell structure and with both pH-responsive and surface charge switchable properties. Spherical composite nanoparticles have been successfully fabricated through a modified emulsion-gelation method with a controllable size (316-573 nm), surface charge (-27.6 to 31.75 mV) and encapsulation efficiency up to 70.8%. The dilemma can be avoided by tailoring the composite nanoparticles with the specially designed core-shell structure to be negative charged in the beginning and switch to positive charge later on. The negative charge of particles can be switched to positive charge gradually as the erosion of biodegradable polymer shells and exposure of the positive charged chitosan core. The formed chitosan hydrogel exhibited multi-layer structures, which

were primarily influenced by chitosan concentration. Influences of the chitosan gelation behaviors on the properties of the composite nanoparticles in response to different chitosan and NH_3 concentrations have also been studied. Release rate decreased significantly with increasing chitosan concentration. With the introduction of the chitosan, the increase in drug release rate by orders of magnitude was observed for the samples immersing in the phosphate buffer saline solution of lower pH value proving a pH responsive release property. Drug release profiles of the composite nanoparticles can be divided into fast release stage and slow release stage. The fast release stage was well described by a modified first-order kinetic model; while the slow release stage was fitted well with the classical first-order release kinetic model. All the presented results make the proposed composite nanoparticles a promising system for controlled drug delivery.

Keywords: A. Polymer-matrix composites (PMCs); A. Nano-structures; A. Particle-reinforcement; B. Microstructures; Chitosan; Surface charge

1. Introduction

Polymer nanoparticles with targeting capability have been widely developed as promising drug delivery vehicles [1-3]. Enhanced disease tissue accumulation and cellar internalization are two basic properties for nanoparticles to have achieved target delivery [4-6]. Tumor accumulation is usually achieved through a long circulation time and the permeability and retention (EPR) effect, which allows nanoparticles to

penetrate through the leaky tumor vasculature other than normal tissue in a passive way [7-8]. Cellular internalization is another important step for the accumulated nanoparticles to have efficacious therapeutic results, which is associated with the size and surface properties of nanoparticles [9]. The internalization process is usually enhanced by grafting targeting ligands or the positive charged surfaces of nanoparticles, since these decorations on the particle surfaces can induce the ligand-receptor interactions or electrostatic interactions with cell membranes [10]. It has been discovered that positive charged or ligand decorated nanoparticles are generally easy to be recognized and cleared by the reticuloendothelial system (RES), which can significantly reduce the circulation time and thus deteriorate the accumulation of nanoparticles on tumor sites [11]. Prolonged circulation time and enhanced accumulation can be achieved by adopting negatively charged nanoparticles modified with hydrophilic groups, such as PEG, on their surfaces [12]. However, the negative charge and hydrophilic groups could hinder the interactions between nanoparticles and cell membrane, which is unfavorable for cellular interaction [13].

In order to solve this dilemma, nanoparticles with switchable surface properties are desirable. Nanoparticles are required to exhibit a negative charge before reaching tumor sites. After their accumulation on the tumor tissues, the nanoparticles are required to become positively charged in order to accelerate the cellular internalization. To realize this delivery strategy, some attempts have been employed to develop surface charge-switchable nanoparticles [7]. Hung et al. [14] developed a pH-triggered surface charge-

switchable poly (lactide-co-glycolide) (PLGA) nanoparticles for drug delivery by grafting pH-responsive N-acetyl histidine modified D-α-tocopheryl polyethylene glycol succinate chains on the surface of the PLGA nanoparticles. These modified PLGA nanoparticles changed to be positively charged after being triggered by acid tumor extracellular environment due to the enhanced protonation of the grafted functional groups. In another study, negatively charged 2, 3-dimethylmaleic anhydride (DMMA) groups were introduced to shield the positively charged nanoparticles by binding them with the amino groups on the particle surfaces [15]. The DMMA groups detached from the amino groups responding to the tumor extracellular acidity would recover to become positively charged. Another strategy to achieve surface charge switching is the adoption of the Zwitterionic surfaces [16-18]. A variety of pH-responsive zwitterionic groups have been developed for the surface modification of nanoparticles, such as carboxybetaine[16], phosphorylcholine[17] and alkoxyphenyl acylsulfonaminde[18]. These functional groups are capable to switch from negative or natural charges to positive charges at acidic environments. Thus, this type of surface modification has been proved to be an effective route to equip nanoparticles with a surface charge switching property. However, these surface modification processes are usually complex and may deteriorate the nanoparticles in certain extend.

PLGA, an American food and drug administration (FDA) approved polymer, has attracted increasing attention as the primary composition of nanoparticles for drug delivery purpose, because of its degradability and controllable drug release profile [1,

8, 19-21]. However, the negatively charged surfaces of PLGA based nanoparticles render them inappropriate to have effective targeting effects. Chitosan, a natural occurring biodegradable polymer acquired from the deacetylation of chitin, has been widely adopted in industrial and pharmaceutical applications, because of its intrinsic properties such as biocompatibility, biodegradability, bacteriostatic effect and abundance in nature [1, 22-25]. The positive charges of chitosan based nanoparticles are beneficial for cell affinity and internalization. However, the circulation time is compromised.

In this study, with motivation by the merits of both polymers, we have designed a novel and facile strategy for fabricating effective pH-responsive and switchable surface charged chitosan hydrogel/PLGA core-shell composite nanoparticles for drug delivery. A model drug, vancomycin HCl, was incorporated into the pH-responsive chitosan hydrogel core which was then encapsulated by the PLGA shell through a one-step emulsion gelation method. With the developed core-shell structure, the positively charged chitosan could be physically shielded. Following the erosion of the polymer shell and the exposure of chitosan core, the surface properties of the composite nanoparticles were switched from negative to positive charges. Gelation behaviors of the chitosan solution in response to the concentration of chitosan and alkali were studied. Influences of key process parameters on the particle size, drug encapsulation efficiency, surface charge and drug release kinetics of the composite nanoparticles were all investigated.

2. Material and methods

2.1 Materials

Poly (lactic-co-glycolic acid) (PLGA) (Mw: ~30kDa) and Poly ((D, L-lactic acid-co-glycolic acid)-block-ethylene glycol) (PLGA-PEG) (Mw: ~11kDa) were obtained from the Jinan Daigang Biomaterial Co., Ltd. Dichloromethane (DCM), acetate acid and NH_3 solution were purchased from the Merck & Co. Polyvinyl alcohol (Mw: ~23kDa) and tetraethylorthosilicate (TEOS) were acquired from the Sigma-Aldrich. Vancomycin HCl (VCM) was obtained from the Amresco. Chitosan (Mw=~500kDa, deacetylation degree, > 95%) was purchased from the Heifei Bomei Biotechnology Co., Ltd.

2.2 Fabrication of drug loaded Chitosan/PLGA composite Nanoparticles

The proposed composite nanoparticles were prepared through a modified gelation emulsion method [26]. Briefly, 30mg of VCM was dissolved into 1 ml of chitosan solution. Chitosan solutions of different concentration (0.5%-2%) were prepared by dissolving the chitosan powder into acetate acid aqueous solution of the same concentration. 1 ml of the chitosan-VCM solution and 0.1 ml of NH_3 solution were ultrasonically emulsified into 5 ml of PLGA/DCM solution separately to form two emulsions. The PLGA/DCM solution was prepared by dissolving PLGA and PEG-PLGA with a weight ratio of 3 : 2 into 5 ml of DCM. Both of the emulsions were blended and sonicated for 3 minutes to give a primary emulsion. The primary emulsion was then ultrasonically dispersed into 22 mL of 0.5% PVA solution to form the secondary emulsion which was then agitated for 3 hours to evaporate all the organic

solvent. The nanoparticle suspension was centrifuged at 12000 rpm for 30 minutes. The supernatants were kept for drug concentration analysis. The composite nanoparticles were obtained after washing and drying the precipitated solids.

2.3 Characterization

The morphologies and structures of the composite nanoparticles were examined using scanning electron microscopy (SEM) (JEOL JSM-6490) and STEM (JEOL JEM-2100F). Specimens for SEM were treated by coating a gold layer. Compositional information on the nanoparticles was obtained by Fourier Transform Infrared (FTIR) spectrometry (Thermo Scientific Nicolet IS50). The size and zeta potential of the nanoparticles were measured by a Zetasizer Nano ZS (Malvern Instruments, Malvern, U.K.) instrument.

2.4 Determination of Encapsulation efficiency

The concentration of VCM in the supernatant was identified by measuring its absorbance using the UV spectrophotometry at 280.5 nm. A standard curve, that was used to calibrate the relationship between the drug concentration and UV absorbance, was prepared using a drug concentration of 0.6 ~ 0.032 mg/ml in 0.5% of PVA. The standard curve of drug concentration in response to UV absorbance was determined to be $y = 0.16672x\text{-}0.00421$ with a correlation factor R^2 of 0.999 in regression analysis. The encapsulation efficiency (EE) of the vancomycin in the nanoparticles was determined by identifying the concentration of the non-encapsulated free drug in the

supernatant after centrifugation of the nanoparticle suspension at 12000 rpm for 30 minutes. The EE of the drug loaded nanoparticles was calculated by using the following equation:

$$Encapsulation\ Efficiency\ (\%) = \frac{Total\ drug\ amount - Free\ drug\ amount}{Total\ drug\ amount} \times 100\%$$

2.5 In vitro drug release

An appropriate amount of nanoparticles containing 3 mg of VCM were dispersed into 40 ml of phosphate buffer solution (PBS) (pH = 7.2 ± 0.2) in a 50 ml tube with a cap. The tube was shaken at 100 cycles/min in a gas bath shaker with a constant temperature of 37.0 ± 0.2 °C. 4 ml of dissolution medium was withdrawn from each tube at a fixed time interval. After centrifugation at 12000 rpm for 10 minutes, 2 ml of supernatants of the collected dissolution medium samples were filtered through 0.22μm membrane before analyzing the drug concentration via UV/vis spectrophotometry at 280.5 nm. All the dissolution mediums were added back to the corresponding tube after the completion of analysis.

3. Results and Discussion

3.1 Size, morphology, encapsulation efficiency and zeta potential of the composite nanoparticles

Composite nanoparticles prepared with 1% of chitosan and 1.5% NH_3 concentration in this study were spherical as confirmed in the SEM image in Fig.1(a), and their particle size distribution was acceptable with a low polydispersity index of 0.262. For the

composite nanoparticles prepared with 1% of chitosan concentration, their size increases up to 413 nm with increasing NH_3 concentration from 0.75% to 3%, while there is a decrease in the particle size up to 367 nm for the NH_3 concentration of 3% ~ 12% as shown in Fig.2. From Fig.3, the particle size increases from 404 to 573 nm with decreasing chitosan concentration from 2% to 0.063% for a constant ratio of chitosan to NH_3 concentration. It can also be observed from Fig.2 that the particle size and surface charge (zeta potential) of the composite nanoparticles rise with the NH_3 concentration before 3% NH_3 concentration. The particle size exhibits only a mild decrease when the NH_3 concentration is above 6%, which is due to the formation of more compact hydrogel in the presence of the extra alkali. With different chitosan and NH_3 concentrations, encapsulation efficiency (EE) and Zeta potential also vary from 56.1% to 70.8% and -27.6 to 31.75 mV respectively (Figs.2&3). All these results are further discussed in the following sections.

3.2 FT-IR analysis

The comparative FI-IR spectrum of PLGA, chitosan, PEG-PLGA and composite nanoparticles is presented in Fig.4. The strong peak at 1755 cm^{-1} is assigned to the stretching vibration of the ester C=O of PLGA and PEG-PLGA. The asymmetric and symmetric stretching vibration of the C-H bonds of $–CH_3$ groups of the PLGA and PEG-PLGA are characterized by the peaks at 3003 cm^{-1} and 2955 cm^{-1} respectively. The peak at 2883 cm^{-1} is due to the C-H stretching vibration of $-CH_2$. The characteristic peaks at 1645 cm^{-1} and 1598 cm^{-1} are the N-H bending vibration of the primary and

secondary amides of chitosan respectively, confirming the presence of chitosan in the composite nanoparticles. The stretching vibrations of N-H and O-H groups of chitosan are expressed as the wide and sharp peak at 3480 cm^{-1} in Fig.4 (d). The peaks at ~3480 cm^{-1} of the PLGA and PEG-PLGA are associated with the –OH stretching vibration.

3.3 Investigation on gelation process of chitosan solution

The chitosan solution in this study was physically gelled by the exposure to alkali, leading to the entanglement of the chitosan molecular chains. Referring to our fabrication process, the chitosan solution and NH_3 solution were firstly dispersed into the individual PLGA/DCM solution. The gelation of the chitosan solution droplets was triggered by their collisions with the droplets of NH_3 solution. The collisions may occur between two different droplets or among multiple droplets as confirmed in TEM image (Fig.5 (a) & (b)). After collision, the NH_3 solution droplets start to merge with the chitosan solution as shown in Fig.5(c). According to Fick's first law, the solute (NH_3) diffused from a high concentration region (NH_3 droplet) to a low concentration region (chitosan droplet) across a concentration gradient.

This gradient diffusion of the alkali solution has been found to enable formation of multilayer chitosan hydrogel instead of forming cross-linked gel simultaneously as reported in literature [27]. According to their study, the gelation speed of the chitosan solution decreased while the alkali solution diffused from the top to the bottom, leading to formation of multilayer chitosan hydrogel with different structure. A primary

chitosan hydrogel layer with a smooth and compact structure was formed promptly on the interface once in contact with the alkali solution. Following the continuous diffusion of alkali solution to the bottom, an oriented layer, which is characterized by a diffusion direction oriented structure with minor porosity, was formed. In this layer, some of the chitosan molecular chains was deprotonated and embed in the upper unit, while the other part of the chains were relaxed and able to interact with other unrestricted protonated molecular chains. Due to the diffusion of the alkali solution, the relaxed part of the molecular chains was restricted and the chitosan molecular chains interacting with this part of the chains was therefore aligned. This orientation has been found to occur only in the high chitosan concentration. It was also found that there was a critical chitosan concentration below which the orientation layer could not be formed. The viscosity of the chitosan solution for its concentration above and below the critical values was found to vary significantly. This critical chitosan concentration was found to be reduced with increasing molecular weight of the chitosan. A highly porous layer was formed in the highly reduced alkali solution or in the chitosan solution with the concentration below its critical value, which was considered to be isotropic.

In the current study, the alkali (NH_3) droplet diffused from its center towards outward. The generated chitosan hydrogel core was assumed to have a multi-layer structure following the similar gelation process as discussed above. As illustrated in Fig.6, there should be a compact, oriented and porous structure and unreacted chitosan along the diffusion direction of the NH_3 droplets. Thus, the gelation behaviors of the chitosan

solution and the properties of the composite nanoparticles became highly dependent on the concentration of the chitosan and NH_3 solutions.

3.4 Control and influences of the gelation behavior of chitosan

The critical polymer concentration has been discovered to be 0.56wt.% for the chitosan of molecular weight of 200kDa as reported in literature[27]. Since the molecular weight of the chitosan in the present study is about 500kDa, the critical concentration should be lower than 0.56 wt.%. A series of the chitosan concentrations ranging from 0.0625 to 2.0wt.% were therefore adopted to determine its critical concentration, and explore the properties changes of the composite nanoparticles around this critical concentration. From Fig.3, the critical chitosan concentration was found to be 0.37 wt.%, as reflected from the most remarkable change of the particle size over other properties. It can also be observed from this figure that the particle size exhibits an insignificant decrease with increasing chitosan concentration above the critical value, but increases significantly for the chitosan concentration below the critical value. As discussed in Section 3.3, most of the chitosan gel had a highly porous structure, because the oriented layer was rarely formed when the chitosan solution was below the critical value. Moreover, this porous structure could encapsulate and prevent the outflow of more water molecules as well as drug molecules as compared with the less porous oriented layer. This result has been confirmed by the increasing tendency of EE with the decrease of chitosan concentration, especially when the concentration is below the critical value (Fig.3). Surface properties of the composite nanoparticles, in terms of surface charge, exhibited a proportional

relationship with the chitosan concentration, which is primarily ascribed to the reducing content of positively charged chitosan in the nanoparticles. It was because the surface charge of the nanoparticles changed from a negative to positive one due to the introduction of the chitosan as the core material. This charge change may result from partially protonated chitosan molecular chains tending to penetrate through the polymer shell and influence the charge balance of the particles; while the deprotonated part of the chitosan chains was embedded in the hydrogel matrix of the particle core. The amount of the added alkali (NH_3) solution was just enough to neutralize acetate acid in each formulation of the samples in Fig.3. The protonated chitosan molecules at the surface of hydrogel core were supposed to be deprotonated by the addition of extra alkali, which could therefore change the charge of the particles. To verify this assumption, different NH_3 concentrations were adopted for preparation of composite nanoparticles containing 1% chitosan solution.

Referring to the results depicted in Fig.2 and described in section 3.1, 3% NH_3 concentration was just enough to cause gelation of the nanoparticles by neutralizing all the acid in the 1% chitosan concentration. It was because the chitosan solution could not be gelled or deprotonated completely when the NH_3 concentration is below 3%). The unrestricted protonated (unreacted) chitosan molecules tended to escape from the nanoparticles under sonication during fabrication process, leading to the reduction of particle size with decreasing NH_3 concentration. The surface charge of the composite nanoparticles switched from a positive to a negative charge one as in Fig.2 when the

extra NH_3 (with concentration > 3%) was introduced. This result confirmed the previous assumption that the protonated part of the chitosan could be deprotonated and restricted when the extra alkali was used. From Fig.2, a further increase of the NH_3 concentration (>3%) would lead to formation of less unrestricted and protonated chitosan molecular chains. The impact of the positively charged chitosan on the negatively charged polymer shell was therefore minimized. Zeta potential of composite nanoparticles decreases slightly in a lower NH_3 concentration (< 3%) as in Fig.2 owing to the leakage of the protonated and free chitosan molecules during fabrication. The composite nanoparticles with a negative charge can be switched to possess a positive charge, when the cores of the drug loaded chitosan were exposed to the body fluid after erosion of its polymeric shells. This equips the nanoparticles with advantageous properties of both long circulation time and good cell affinity.

3.5 In vitro drug release kinetic

Drug release profiles of composite nanoparticles prepared with chitosan concentrations ranging from 0.25% to 2% are presented in Fig.7. Drug releases within 24 hours and 2 weeks vary from 83% to 48% and 95% to 68% respectively with increasing chitosan concentration up to 2%. Because of the core-shell structure of the composite nanoparticles, the drug molecules released from the chitosan core were influenced by the erosion of polymeric shells, degradation of the chitosan, dissolution and diffusion of the drug molecules. The drug release profiles of the composite nanoparticles were approximated by two stages: an initial fast release stage within the first 24 hours and a

subsequent sustained slow release stage. The first release stage resulted from a combinational effect of dissolution and diffusion of the drug molecules that were embedded in the polymeric shell and entrapped in the porous layer of the chitosan core. The release profiles of the first stage release reflected the diffusion controlled dissolution of the embedded drugs. After most of the drug molecules embedded in polymeric shell and the porous structure of the chitosan hydrogel core were released within the first 24 hours, the release rate of the entire system became reduced significantly. According to the characteristics of the fast release stage, the cumulative release at any time during the first 24 hours could be approximated to be the upper limit (A) of the fast release stage. This release behavior could be characterized by the following equation developed based on the first-order kinetics [28] modified with an additional upper limit, A.

$$\frac{M_t}{M_\infty} = A(1 - e^{-kt}) \quad (1)$$

where M_t and M_∞ are defined as fractions of the released drugs at time t and infinite time respectively; k is the release rate constant. This modified first order kinetic would become classic first-order kinetic when A is equal to 1. Therefore, equation (1) is applied to characterize the situations when A is not equal to 1,

Regression analysis of the data was performed using the equation (1) and the results are shown in Table 1. The release rate constant (k) increases gradually with reducing chitosan concentration, especially when the concentration is lower than 0.5% (Fig.8). This result is coincident with the relationship between the chitosan concentration and

formation of the porous layer as described in Section 3.3. Comparison between the predicted and experimental values of A is presented in Table 1 and Fig.9. The relative errors of between predicted and experimental A values were found to be smaller than 7%, with no significant difference as confirmed in a student t test with $p < 0.05$. All these analysis results have confirmed the effectiveness of the equation (1) in describing the drug release kinetics of the composite nanoparticles in the fast release stage.

The following slow release stage may be ascribed to the combinational effects of the erosion of polymer shells, erosion of chitosan matrices, dissolution and diffusion of the drug molecules encapsulated in the oriented and compact structures of the chitosan hydrogel cores. Erosion of the polymer shells and chitosan matrices were assumed to be the dominating effects, because the drug molecules encapsulated in the chitosan cores, before releasing to the external PBS, were required to penetrate through the eroded polymer shell and chitosan matrices. To investigate this combinational effect, several release kinetics were investigated. Drug release from biodegradable PLGA are usually characterized by the classical first-order kinetics considering the hydrolytic degradation behaviors of polymers [28], which can be expressed by equation (1) with A =1.

Drug released from chitosan nanoparticle was found to be best fitted with the Higuchi square root of time model [29, 30]:

$$\left(\frac{M_t}{M_\infty}\right)^2 = kt \qquad (2)$$

As shown in Fig.7(c), the release profiles exhibit a linear relationship, which is usually described by the zero order release kinetics [31]:

$$\frac{M_t}{M_\infty} = kt \tag{3}$$

To evaluate the effectiveness of these models, regression analysis was performed by fitting the data by various the kinetics models. Correlation coefficients (R) of the aforesaid models are compared in Table 2. The first order kinetics show the best fit with the cumulative release data for the slow release stage. From Fig.10, the release rate constant (k) at 0.25% chitosan concentration is 5 times greater than that of higher chitosan concentration due to the absence of the oriented structure in the chitosan with a concentration lower than its critical value of 0.37%.

Influences of external stimuli, in terms of pH value, on drug release profiles of the drug loaded composite nanoparticles were evaluated by immersing the samples in PBS solution with different pH values. As shown in Fig.11, a significant increase for the drug release rate of the nanoparticles is observed for the samples in the PBS solution of lower pH value. The samples in the PBS solution of pH=1.2 exhibits the fastest release rate and realize 100% release in 5 days; but the sample in the PBS solution of pH=4.8 shows a complete release in 14 days. Regression analyses of the fast release stage and slow release stage were performed by using the modified first-order kinetic ($A \neq 1$) and the classical first-order kinetic ($A=1$) equations, respectively (Table 3). For the fast release stage, a relatively mild increase in the release rate with reducing pH values is

observed, because the erosion of polymeric shell in this stage was relatively less impacted by the pH value of PBS solution. For the slow release stage, the increase in the release rate becomes more significant as shown in Fig.11(c), because the primary effect of the second stage release is the swelling and degradation behavior of the chitosan which is significantly influenced by the pH value. As the chitosan molecular chains were protonated in a lower pH solution, it led to the swelling and dissolution behaviors, and contributed to the fast release rate of the encapsulated drugs.

Conclusion

Surface charge switchable and pH responsive vancomycin loaded chitosan/polymer composite nanoparticles of a novel core-shell structure with an adjustable size range of 316-573 nm and a drug encapsulation efficiency up to 70.8% have been successfully fabricated in the first attempt via a modified gelation emulsion method. Surface charges of the particles could be controlled from -27.6 to 31.75 mV by adjusting the concentrations of the chitosan and NH_3 solutions. The conflicts of long circulation time and good cell affinity could be avoided by developing negatively charged composite nanoparticles, because the exposure of the chitosan core after degradation of the polymer shells could switch the nanoparticles to possess a positive charge. The generated chitosan hydrogel core exhibited multi-layer structures with a combination of compact layer, oriented layer and highly porous layer along the diffusion direction of the incorporated NH_3 solution, which have been found to influence the properties of composite nanoparticles. Formation of multilayer chitosan hydrogel was found to be

related to the concentration of chitosan solution. The critical chitosan concentration was confirmed to be 0.37%, below which no oriented structure was formed. Moreover, influences of the gelation behaviors of chitosan solution on the size, zeta potential, encapsulation efficiency as well as drug release were well investigated. Drug release profiles of the nanoparticles were classified into a fast release stage (≤ 24 hours) and a slow release stage (> 24 hours). The fast release stage was caused by the diffusion controlled dissolution behaviors of drug molecules embedded in the polymeric shell and the porous structure of the chitosan core, which exhibited modified first-order release kinetics. The slow release stage was attributed to the erosion of polymer shells and chitosan cores of the nanoparticles, which was found to follow the classical first-order release kinetics. In addition, the release rates (slow release stage) of the composite nanoparticles were accelerated by two orders of magnitude in a PBS solution with a pH value reduced from 7.4 to 1.2, which confirmed the pH-response functions of the proposed composite nanoparticles that are applicable for effective treatment of the disease cells/tissues with an acid cellular environment.

ACKNOWLEDGMENT

The authors would like to thank the support from the Research Committee of The Hong Kong Polytechnic University (RTE9) for support in this study.

References

[1] Kumari A, Yadav SK, Yadav SC. Biodegradable polymeric nanoparticles based drug delivery systems. Colloids and surfaces B, Biointerfaces. 2010;75(1):1-18.
[2] Patel T, Zhou JB, Piepmeier JM, Saltzman WM. Polymeric nanoparticles for drug

delivery to the central nervous system. Advanced drug delivery reviews. 2012;64(7):701-5.
[3] Couvreur P. Nanoparticles in drug delivery: Past, present and future. Advanced drug delivery reviews. 2013;65(1):21-3.
[4] Sun T, Zhang YS, Pang B, Hyun DC, Yang M, Xia Y. Engineered nanoparticles for drug delivery in cancer therapy. Angewandte Chemie. 2014;53(46):12320-64.
[5] Vasir JK, Labhasetwar V. Biodegradable nanoparticles for cytosolic delivery of therapeutics. Advanced drug delivery reviews. 2007;59(8):718-28.
[6] Brigger I, Dubernet C, Couvreur P. Nanoparticles in cancer therapy and diagnosis. Advanced drug delivery reviews. 2012;64:24-36.
[7] Wang S, Huang P, Chen X. Hierarchical Targeting Strategy for Enhanced Tumor Tissue Accumulation/Retention and Cellular Internalization. Advanced materials. 2016;28(34):7340-64.
[8] Danhier F, Ansorena E, Silva JM, Coco R, Le Breton A, Preat V. PLGA-based nanoparticles: an overview of biomedical applications. Journal of controlled release : official journal of the Controlled Release Society. 2012;161(2):505-22.
[9] Sherlock SP, Tabakman SM, Xie LM, Dai HJ. Photothermally Enhanced Drug Delivery by Ultrasmall Multifunctional FeCo/Graphitic Shell Nanocrystals. Acs Nano. 2011;5(2):1505-12.
[10] Ashley CE, Carnes EC, Phillips GK, Padilla D, Durfee PN, Brown PA, et al. The targeted delivery of multicomponent cargos to cancer cells by nanoporous particle-supported lipid bilayers Nature materials. 2011;10(6):476.
[11] Fang J, Nakamura H, Maeda H. The EPR effect: Unique features of tumor blood vessels for drug delivery, factors involved, and limitations and augmentation of the effect. Advanced drug delivery reviews. 2011;63(3):136-51.
[12] Deng H, Lei Z. Preparation and characterization of hollow Fe3O4/SiO2@PEG–PLA nanoparticles for drug delivery. Composites Part B: Engineering. 2013;54:194-9.
[13] Wang Y, Li P, Kong L. Chitosan-modified PLGA nanoparticles with versatile surface for improved drug delivery. AAPS PharmSciTech. 2013;14(2):585-92.
[14] Hung CC, Huang WC, Lin YW, Yu TW, Chen HH, Lin SC, et al. Active Tumor Permeation and Uptake of Surface Charge-Switchable Theranostic Nanoparticles for Imaging-Guided Photothermal/Chemo Combinatorial Therapy. Theranostics. 2016;6(3):302-17.
[15] Zhang JA, Wu XJ, Wang ZB, Chen Y, Wang X, Zhou M, et al. Fused-Gene Approach to Photoswitchable and Fluorescent Biliproteins. Angew Chem Int Edit. 2010;49(32):5456-8.
[16] Zhang L, Xue H, Gao CL, Carr L, Wang JN, Chu BC, et al. Imaging and cell targeting characteristics of magnetic nanoparticles modified by a functionalizable zwitterionic polymer with adhesive 3,4-dihydroxyphenyl-L-alanine linkages. Biomaterials. 2010;31(25):6582-8.
[17] Jin Q, Xu JP, Ji J, Shen JC. Zwitterionic phosphorylcholine as a better ligand for stabilizing large biocompatible gold nanoparticles. Chemical communications. 2008(26):3058-60.

[18] Mizuhara T, Saha K, Moyano DF, Kim CS, Yan B, Kim YK, et al. Acylsulfonamide-Functionalized Zwitterionic Gold Nanoparticles for Enhanced Cellular Uptake at Tumor pH. Angew Chem Int Edit. 2015;54(22):6567-70.
[19] Panyam J, Labhasetwar V. Biodegradable nanoparticles for drug and gene delivery to cells and tissue. Advanced drug delivery reviews. 2012;64:61-71.
[20] Gomes ME, Reis RL. Biodegradable polymers and composites in biomedical applications: from catgut to tissue engineering. Part 2 Systems for temporary replacement and advanced tissue regeneration. International Materials Reviews. 2004;49(5):274-85.
[21] Tudorachi N, Chiriac AP, Mustata F. New nanocomposite based on poly(lactic-co-glycolic acid) copolymer and magnetite. Synthesis and characterization. Composites Part B: Engineering. 2015;72:150-9.
[22] Ionita M, Iovu H, Mechanical properties, urea diffusion, and cell cultural response of poly(vinyl alcohol)–Chitosan bioartificial membranes via molecular modelling and experimental investigation, Composites Part B: Engineering, 2012;43:2464-70.
[23] Xu KM, Li KF, Zhong TH, Guan LT, Xie CP, Li S, Effects of chitosan as biopolymer coupling agent on the thermal and rheological properties of polyvinyl chloride/wood flour composites, Composites Part B: Engineering, 2014;58:392-99.
[24] Râpă M, Miteluţ AC, Tănase EE, Grosu E, Popescu P, Popa ME, Rosnes JT, Sivertsvik M, Darie-Niţă RN, Vasile C, Influence of chitosan on mechanical, thermal, barrier and antimicrobial properties of PLA-biocomposites for food packaging, Composites Part B: Engineering, 2016;102:112-21.
[25] Nikpour MR, Rabiee SM, Jahanshahi M. Synthesis and characterization of hydroxyapatite/chitosan nanocomposite materials for medical engineering applications. Composites Part B: Engineering. 2012;43(4):1881-6.
[26] Huang WF, Tsui GCP, Tang CY, Yang M. Fabrication and process investigation of vancomycin loaded silica xerogel/polymer core–shell composite nanoparticles for drug delivery. Composites Part B: Engineering. 2016;95:272-81.
[27] Nie J, Lu W, Ma J, Yang L, Wang Z, Qin A, et al. Orientation in multi-layer chitosan hydrogel: morphology, mechanism, and design principle. Scientific reports. 2015;5:7635.
[28] Korber M. PLGA erosion: solubility- or diffusion-controlled? Pharmaceutical research. 2010;27(11):2414-20.
[29] Higuchi T. Mechanism of sustained action medication: theoretical analysis of rate of release of solid drugs dispersed in solid matrices. Journal of pharmaceutical sciences. 1963;52:1145-9.
[30] Adlin Jino Nesalin J, Anton Smith A. Preparation and evaluation of stavudine loaded chitosan nanoparticles. Journal of Pharmacy Research. 2013;6(2):268-74.
[31] Kockisch S, Rees GD, Tsibouklis J, Smart JD. Mucoadhesive, triclosan-loaded polymer microspheres for application to the oral cavity: preparation and controlled release characteristics. European journal of pharmaceutics and biopharmaceutics : official journal of Arbeitsgemeinschaft fur Pharmazeutische Verfahrenstechnik eV. 2005;59(1):207-16.

Figures

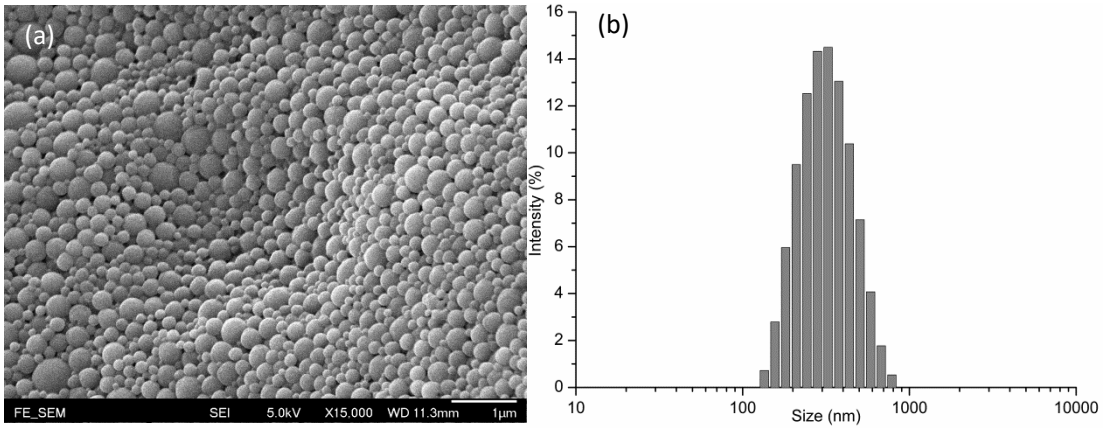

Fig.1 Composite nanoparticles prepared with 1% of chitosan and 1.5% NH_3 concentration (Average diameter: 334 nm, Polydispersity index:0.262), (a) SEM image, and (b) particle size distribution

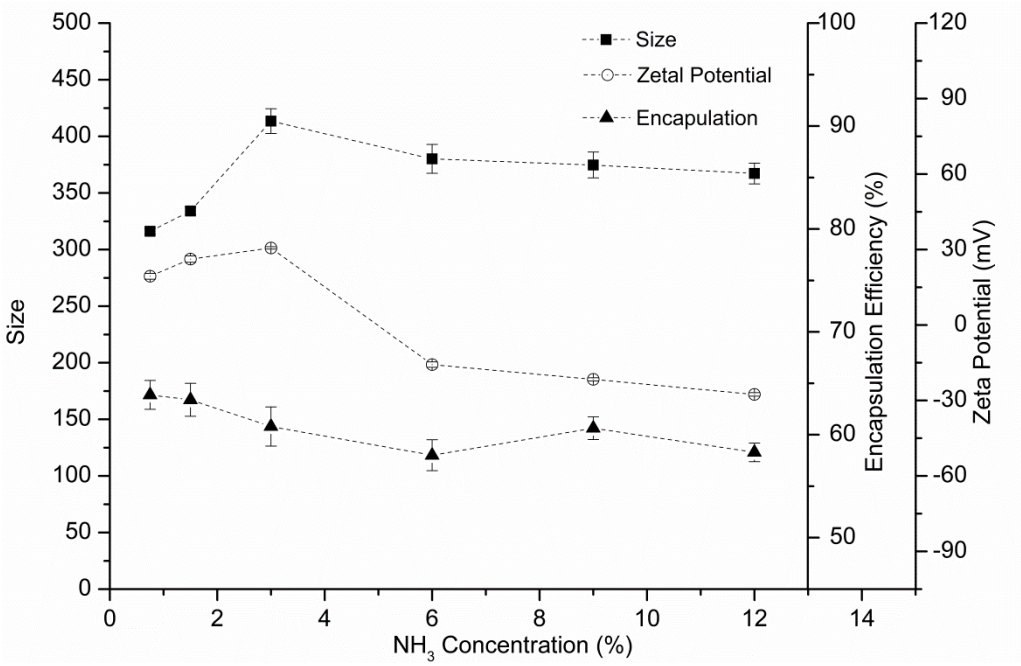

Fig.2 Comparison of composite nanoparticles prepared with different NH_3 concentration and a constant 1% chitosan concentration

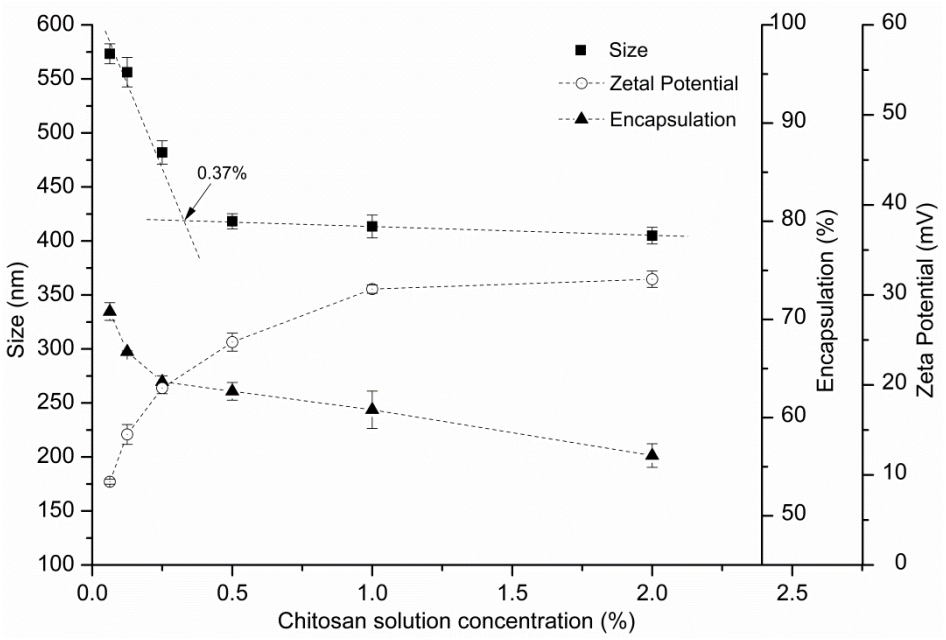

Fig. 3 Comparison of composite nanoparticle prepared with different chitosan concentration at a constant ratio (1:3) of chitosan to NH_3 concentration

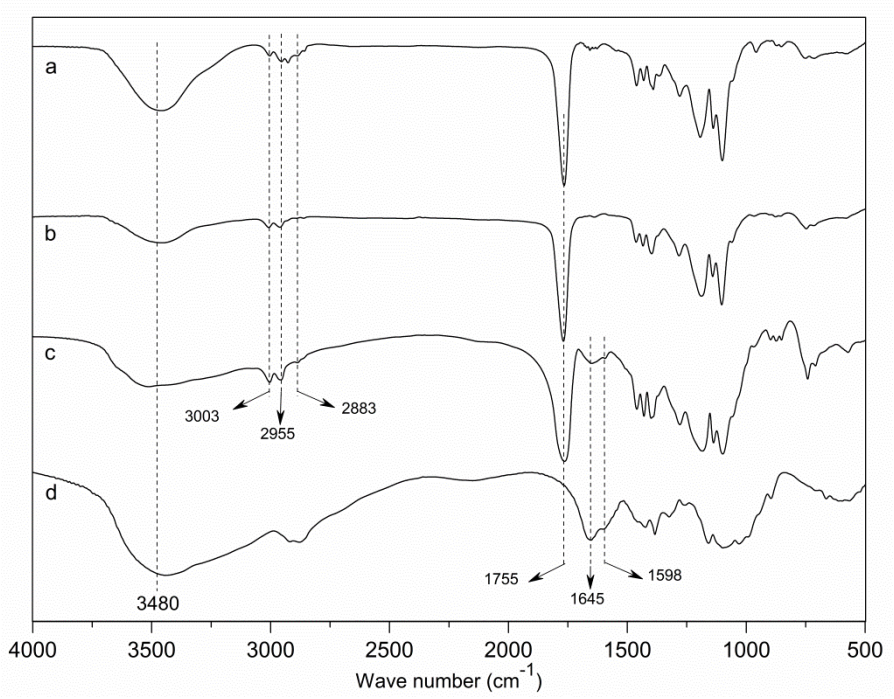

Fig.4 FT-IR spectra of (a) PEG-PLGA, (b) PLGA, (c) composite nanoparticle and (d) chitosan

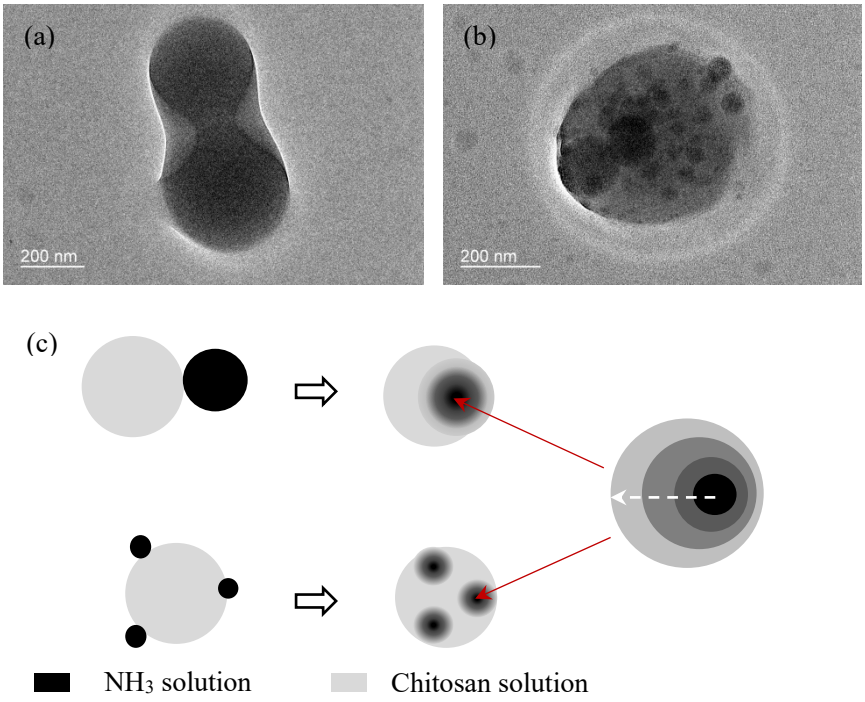

Fig.5 Images and schematic formation of chitosan hydrogel core during fabrication, (a) & (b): TEM images of composite nanoparticles. (c) Schematic integration and diffusion of NH_3 into chitosan droplets.

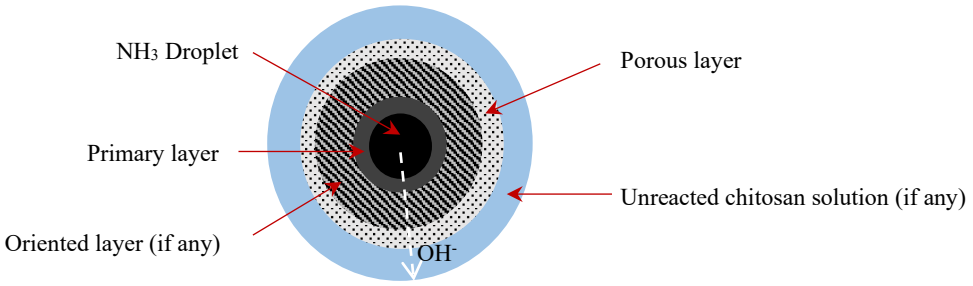

Fig.6 Schematic chitosan core structure

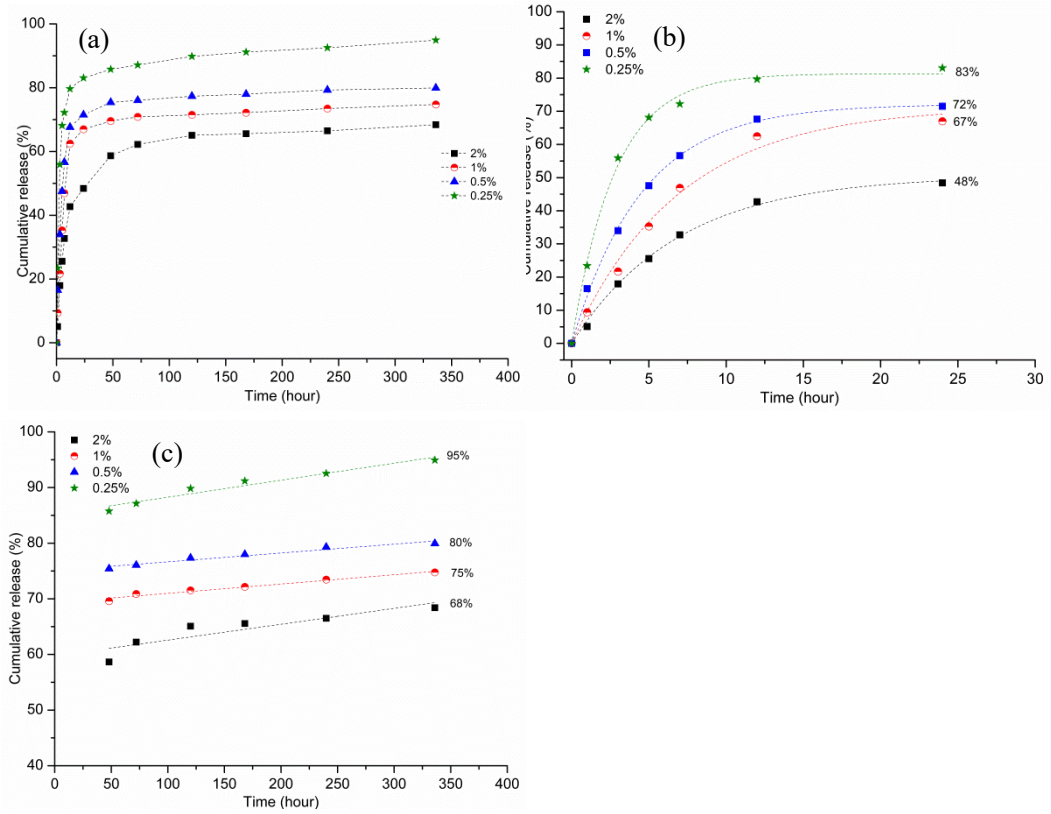

Fig.7 Drug release profiles of composite nanoparticles with various chitosan concentrations under different stages. (a) the entire drug release stage, (b) the fast release stage (≤ 24 hours), and (c) the slow release stage (> 24 hours)

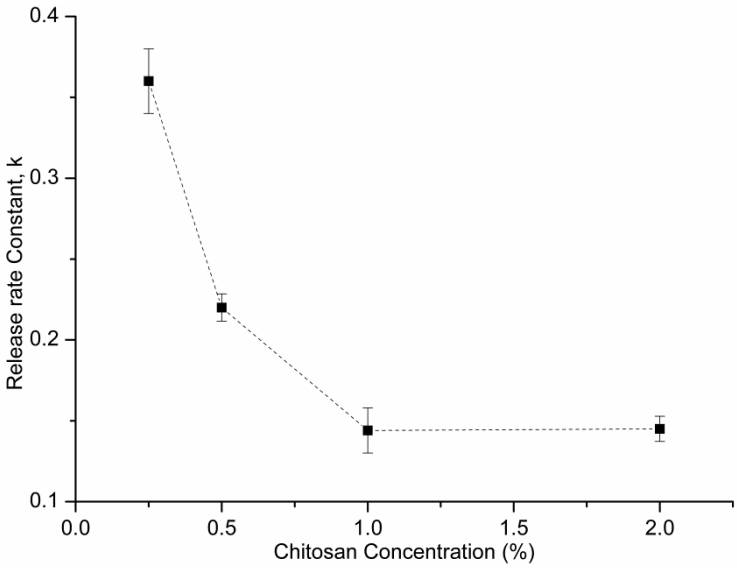

Fig.8. Release rate constants (*k*) for the first release stage with different chitosan concentrations (pH=7.4)

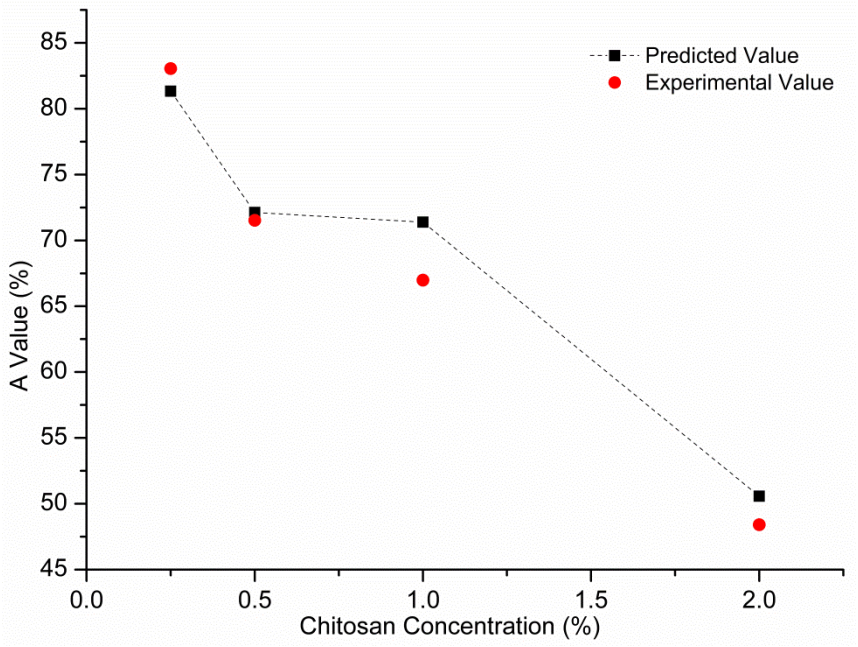

Fig.9 Comparision of predicted and experimental release upper limit (*A*) values

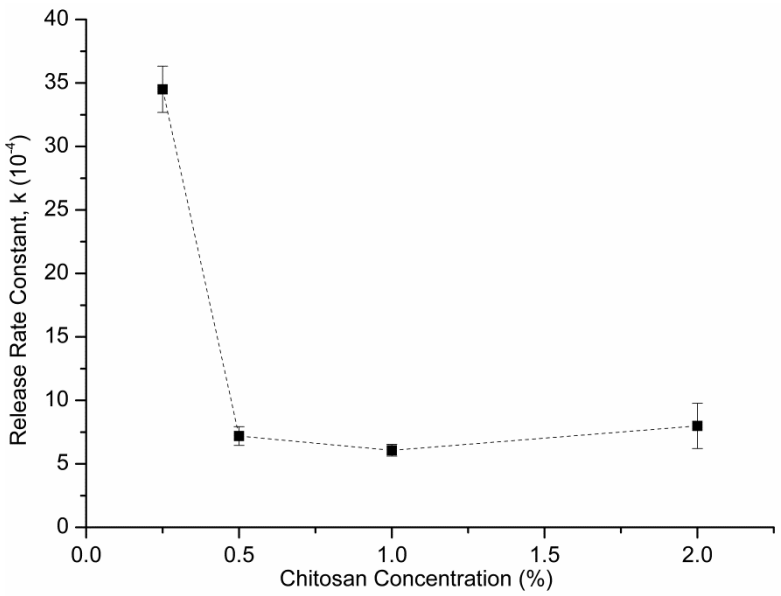

Fig.10 Release rate constants (*k*) for the slow release stage with different chitosan concentrations (pH=7.4)

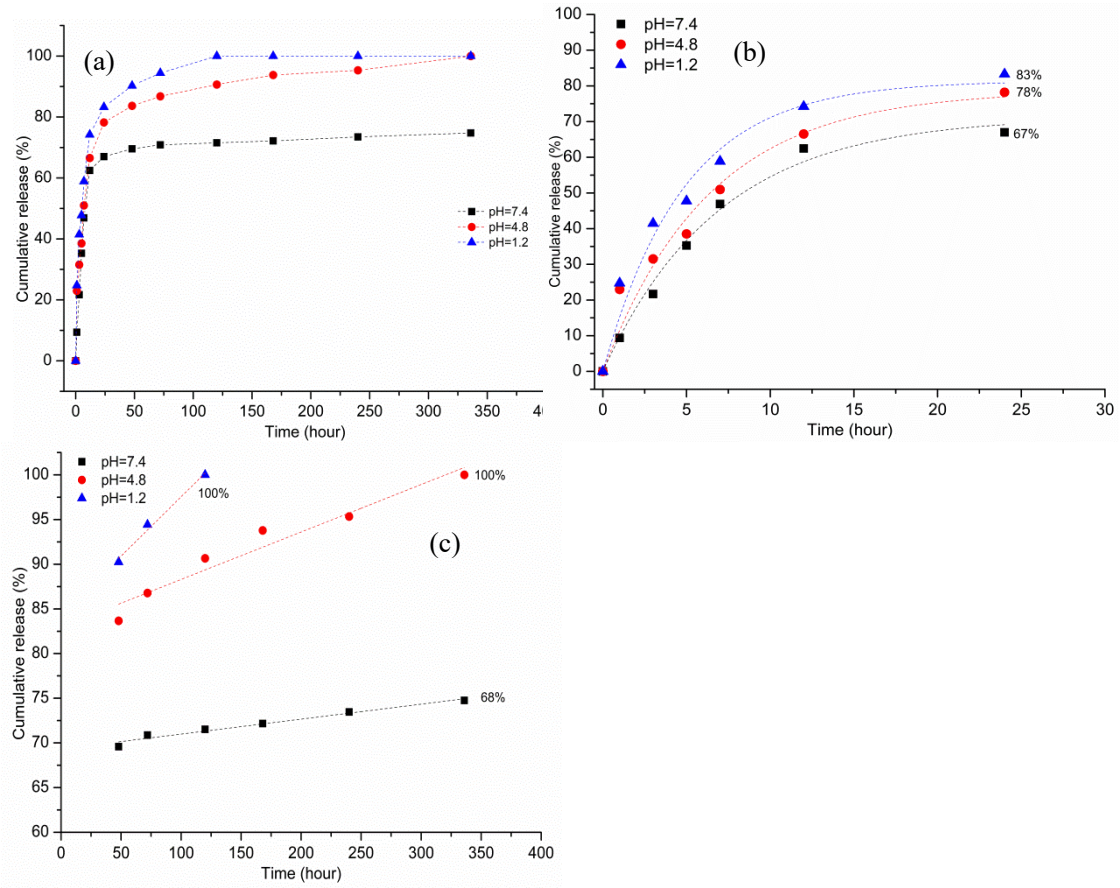

Fig.11 Drug release profiles of composite nanoparticles with 1% chitosan concentrations in PBS of different pH values under different stages. (a) the entire drug release stage, (b) the fast release stage (≤ 24 hours), and (c) the slow release stage (> 24 hours)

Tables

Table 1 Correlation coefficient(R), release rate constant and release upper limit of the modified kinetic model (A≠1)for first release stage.

Parameter	2.00%	1.00%	0.50%	0.25%
Correlation coefficient (*R*)	0.998	0.996	0.999	0.999
k	0.145(±0.0078)	0.144(±0.014)	0.220(±0.0085)	0.360 (±0.020)
Predicted *A*	50.57% (±1.17%)	71.39% (±3.11%)	72.12% (±1.02%)	81.33% (±1.27%)
Experimental *A*	48%	67%	72%	83%

Table 2 Correlation coefficient(*R*) of different release kinetic models for the slow release stage

Model	2.00%	1.00%	0.50%	0.25%
Zero order	0.897	0.985	0.974	0.975
Classical First Order (*A*=1)	0.913	0.989	0.980	0.995
Higuchi	0.906	0.987	0.976	0.978

Table 3 Regression results of samples in PBS solutions with different pH values

Parameter	pH=7.4	pH=4.8	pH=1.2
Fast release stage	0.996	0.981	0.985
k	0.144(±0.014)	0.157(±0.030)	0.207(±0.034)
Slow release stage	0.989	0.989	1
***k* (10^{-4})**	6.07 (±0.46)	66.5(±5.62)	233.2